Gravity balanced compliant shell mechanisms

Radaelli, G.; Herder, J. L.

DOI
10.1016/j.ijsolstr.2017.04.021

Publication date
2017

Document Version
Accepted author manuscript

Published in
International Journal of Solids and Structures

Link to formal publication "International Journal of Solids and Structutures" (Elsevier): https://doi.org/10.1016/j.ijsolstr.2017.04.021

Gravity balanced compliant shell mechanisms

G. Radaelli[a,b], J.L. Herder[a]

[a] *Dept. Precision and Microsystems Engineering, Delft University of Technology, Delft, 2628 CD, The Netherlands*
[b] *Laevo BV, Delft, 2628 CA, The Netherlands*

Abstract

The research on *compliant shell mechanisms* is a new and promising expansion of the well established compliant mechanisms research area. Benefits of compliant shell mechanisms include being spatial and slender, having organic shapes and their high tailorability of the load-displacement response. This work focusses on the design of a shell with tailored force output at large deformations by means of a shape optimization procedure. The procedure is applied to create a statically balanced mechanism where the self-weight of the shell and an additional payload is balanced by the elastic forces of the deforming shell. The optimization is based on an isogeometric numerical simulation. A physical demonstrator is constructed by vacuum forming a PETG polymer sheet. The result of a force measurement on the prototype shows a good qualitative match, although quantitatively the discrepancies are substantial.

Keywords: Compliant Shell Mechanisms, Compliant Mechanisms, Static Balancing, Gravity Balancing, Constant Force Mechanisms

1. Introduction

Compliant mechanisms (CM) are increasingly popular in multiple fields of application. Designers become ever more familiar with their potential

Email addresses: g.radaelli@tudelft.nl (G. Radaelli), j.l.herder@tudelft.nl (J.L. Herder)

benefits, the most frequently mentioned being low friction, no wear, no need for lubrication, no backlash and easy assembly [1]. Other benefits include easy cleaning and possibly more appealing aesthetics. The last one is relevant in case the product is in close contact with the user and a mechanical look is undesired, e.g. in wearable structures (prostheses, orthoses and exoskeletons), consumer products, but also interactive architectural objects and interactive furniture pieces [2, 3].

To date by far most compliant mechanisms are conceived as planar mechanisms and, moreover, they are deduced from equivalent conventional (rigid body) mechanisms. The design process often consists in finding a compliant mechanism alternative to a given rigid body mechanism function [4]. Also, designers tend to subdivide systems in sub-functions and concatenate compliant sub-systems, which often results in relatively large and complex systems. Another observation is that, currently, many compliant systems are so called lumped-compliant. This means that the flexibility is concentrated at certain spots and that most of the material does not deform significantly. This is emphasized by the extensive use of flexures.

We foresee a growing attention for three-dimensional compliant mechanisms in the near future. This expansion makes sense from a technology point of view: planar CM are extensively being investigated thus the logical next step is towards spatial CM. But also from an application point of view it makes sense: Human-assistive devices and tools ought to act essentially spatially since human motion is often hard to approximate as planar.

For the application as human-assistive devices we focus on shell structures as constitutive elements of spatial compliant mechanisms. Shells are interesting from an application point of view because they can be shaped around a limb, for example. From a functional point of view shells are interesting and challenging at the same time, because of their nonlinear nature with respect to mechanical load bearing. Nonlinear load bearing is a risk if regarded as a failure mode, but a benefit when nonlinear load-displacement responses are intentionally produced by a mechanism. There are many ex-

amples where nonlinear load-displacements are a functional requirement. For this class of mechanisms we will use the term *nonlinear spring* from here on, following the definition given by Jutte [5]: "Nonlinear springs are a class of compliant mechanisms having a defined nonlinear load-displacement function measured at one point on the mechanism".

Seffen [6] defines compliant shell mechanisms as "open, thin-walled, discretely corrugated structures, with flat facets or curved regions of shell interconnected by folds or hinge lines", or elsewhere in the paper "discretely corrugated structures, capable of undergoing large, reversible displacements". It sometimes seems appropriate to broaden this definition by not excluding the more continuous case without corrugations, folds or hinge lines. In a more general definition, namely, a shell is a spatially curved, thin-walled structure, in accordance with Farshad's definition [7]. Therefore, if such a structure is compliant and employed as a mechanism, defined as "a mechanical device used to transfer or transform motion, force, or energy" [8, 9], we can call it a *compliant shell mechanism* .

Howell [1], Jutte [5], Leishmann [10] and Merriam [11] mention prosthetics, artificial implants, MEMS, electronic connectors, gripping devices and human interfaces as groups of possible applications of nonlinear springs. Specific nonlinear elastic response is often also at the basis of metamaterials with peculiar mechanical behavior like negative Poisson's ratio [12] and extreme elastic strain [13], just to name a few.

Another important class of mechanisms of which nonlinear springs are essential components are statically balanced compliant mechanisms (SBCM) [14, 15]. In statically balanced compliant mechanisms parasite forces are neutralized by elastic forces generated by the deflection of the mechanism. Parasite forces are called as such because they either require larger actuators or they result in higher stiffness and eigenfrequencies or they disturb a force signal to be transmitted, e.g., haptic sense in surgical tools [16]. The nature of these forces is usually elastic or gravitational. Examples of the first are the intrinsic stiffness of compliant mechanisms. Applications are

found at both meso-scale [17] and micro-scale [18]. In the second case the parasite force is the self-weight or a fixed payload [19].

A special and frequently encountered type of nonlinear spring is a constant force spring. Although the name seems contradictory with the term "nonlinear", we do consider constant force springs as a class of nonlinear springs. The reason is that the constant force is always confined to a certain range. However, reaching that range from a neutral position (zero force) always involves a nonlinear transition. Constant force springs find their applications in gravity balancing, but also for force regulation [20, 21], overload protection [21], constant force actuation [22] and adaptive robot end-effector operations [23].

Buckling is another nonlinear behavior that designers use more and more to their advantage. In his long list of current and envisioned smart applications for buckling, Hu [24] mentions among others: energy production, energy harvesting, energy dissipation, actuators and micro-optical switching, self-deploying and self-locking. Some examples given in this review, e.g. [25, 26, 27, 28], are three-dimensional, are elastic and have doubly curved zones and can thus in theory be classified as compliant shell mechanisms, or closely related.

We observe an increasing attention in other research fields that are related to compliant shell mechanisms. Lamina emergent mechanisms (LEMs) [29, 30, 31], a subset of orthoplanar mechanisms [32], are among the most relevant and fascinating attempts to make compliant mechanisms spatial. Herein designs that are initially fabricated from planar materials also exhibit motion that emerges out of that plane. In the state of the art, however, these mechanisms are mostly lumped-compliant. Moreover, partly due to their originally flat nature, they mostly consist of flat segments. That means that, even in the emerged configuration, single curved surfaces are scarce and double curved surfaces even more.

Origami mechanisms have drawn quite some attention in the past years as well [33, 34, 35]. Many inspiring designs have been realized that are

clearly spatial in both the shape as the behavior. Seffen [6], Norman [36] and Schenk [37] describe extensively what they call *compliant shells* or *compliant shell mechanisms*. The *hypars* shown by Seffen are examples where curvature is introduced in the shaping process. The facets of these special origami are developable surfaces, i.e. with zero Gaussian curvature, that can be shaped from a flat plate material. The *curved corrugated shells* on the other hand, also shown by Seffen, are examples where the surface is locally double curved.

Norman [36] goes in depth into the behavior of multistable corrugated shells that are mostly prestressed in the manufacturing process. Another example of a special shell that owes its behavior to prestress is the one shown by Seffen [38]. This shell has an infinite range of neutrally stable equilibrium configurations, or, in other words, it is statically balanced.

Pellegrino and his co-workers frequently employ the carpenter's tape as a way to create multi-stable deployable structures [39, 40, 41]. The carpenter's tape is also employed by Vehar [42] as a way to create linkages with variable length links. Here they make use of the fact that the longitudinal curvature of the tape in the bended region is constant, independently from the bending angle.

Most of the work found in literature has been focusing on shapes obtainable from flat sheets of material. The more general type of shape with double curved surfaces in the unstressed state is thus often excluded a priori. This fundamental choice has often been made due to the fabrication process. It is true that it is relatively easy to create a shape from a flat sheet of material, benefiting from the uniformity of the material properties and the availability of many common shaping techniques such as plate bending and rolling. On the other hand, there are manufacturing techniques that are becoming more and more accessible and reliable based on composites and polymers that enable shaping of complex double curved shells, e.g. press forming, automated fibre placement, 3d-printing and thermoforming in general.

From a functional perspective, it is expected that free-form shells of which the shape can be tailored will increase the ability to design specific nonlinear spring behaviors and more general compliant shell mechanism behavior. In previous work by the authors [43] it has been shown that the shape of a clamped-clamped planar prismatic beam has an important influence on its nonlinear load-displacement response. The ability to freely manipulate the shape of the undeformed beam by means of shape optimization made it possible to make a weight balancer out of one single piece. The overall shape change of the beam influences the global stiffness behavior, but at a cross-sectional level the bending and tension stiffness do not change. It is expected that giving a transverse curvature to such a beam, i.e. a thin curved cross-section, increases even more the possibilities of tailoring the nonlinear load-displacement response. This is due to the fact that such cross section shape may change during the changing load conditions.

The goal of this paper is to investigate the applicability of a compliant free-form shell as a nonlinear spring of which the response is tailored by optimizing the shape. The work presented in this paper focuses on the design of a constant force spring, as an example of a nonlinear spring. In this peculiar example the elastic forces of the shell, the weight of the shell and an external weight ought to be balanced over a broad range of motion. This balancing is accomplished intrinsically by specifying the function of the total mechanism (end-function) and not by adding up the sub-functions of the sub-systems that counteract each other. Multiple shapes are presented that are obtained by the shape optimization procedure based on an isogeometric framework [44]. A selected shape was constructed by vacuum forming a PETG sheet and tested to verify the applicability of the results and understand the influences of the chosen production method.

The paper is structured as follows. The Methods section 2 contains a problem description, a description of the numerical model and the design optimization. Section 3 shows the results found by the optimization procedure and a convergence analysis on a selected result. Section 4 describes the

physical realisation, the measurements setup and the test results. Section 5 contains the discussion and section 6 ends the paper with the conclusions.

2. Methods

This section illustrates the choices made about the topology of the system and the limitations imposed on the possible shapes. A physical justification of these choices is provided. Details on the numerical model, the parametrization and the optimization procedure are provided.

2.1. Problem description

2.1.1. Phenomenological expectation

Conceptually, the starting point for the gravity balancer to be designed is a clamped-free beam. Practically this is the simplest topology to start with. One single clamping point and one end effector point at the opposite side, i.e. the free end. This resembles roughly the basic structure of a serial robot with one base and one end-effector.

To obtain a constant force mechanism or gravity balancer it is required for a structure with an initial finite stiffness to exhibit a softening behavior in order to transition to a zero stiffness or constant force region.

In a planar beam configuration with constant cross-section, compression buckling is the most likely cause of softening behavior. That is, transitioning from an initial compression dominated load case to a bending dominated load case.

More generally, stiffness change can be caused by the change in alignment of the beam with the end-effector force. For example, if a beam segment is initially aligned with the end-force it primarily experiences either compression or tension, both relatively stiff configurations. If during deformation the orientation and position of this segment changes so that bending becomes dominant, the total stiffness is softening. The other way around, it is also possible that an initially unaligned segment becomes more aligned during deformation, thus causing a stiffening effect.

With a clamped-clamped planar beam with in-between end-effector another important local softening effect can occur. Namely that the two parts of the beam at the opposite side of the end-effector are initially at a certain distance. This distance can become smaller in the course of the deformation. This is illustrated in figure 1, modified from the results of [43]. For the illustration, regard the cross-section indicated by the dashed line as a combined cross-section (CS1) of the system. In the deformed configuration the total cross-section (CS2) narrows down, thus resulting in a much lower bending stiffness. This effect is not expected in a single clamped free beam because the cross-section remains unchanged.

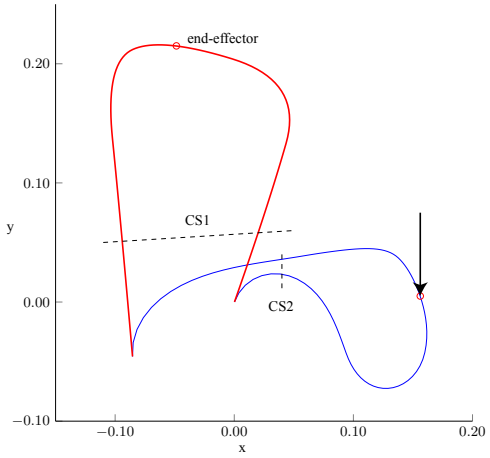

Figure 1: Clamped-clamped planar beam illustrating the softening effect caused by narrowing down of the effective cross-section from CS1 to CS2. Modified results from [43].

However, if the beam's cross-section itself can change shape during deformation, similar softening effects are expected. Think of a carpenter's tape measure. Initially the tension side and the compression side are relatively far apart causing a high second moment of inertia, see figure 2. As the bending load increases, a more favourable deformation state is adopted with small transverse curvature and small total thickness, thus with significantly smaller second moment of inertia. This effect is very localized. In the general case the cross-section is not necessarily constant throughout the

length of the beam, as opposed to the carpenter's tape case. On a global

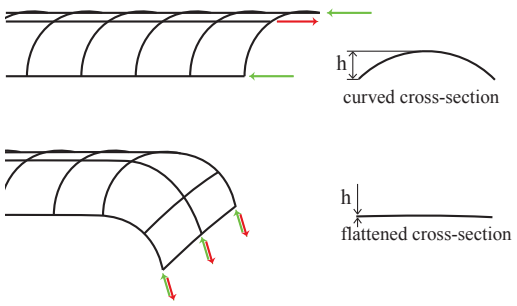

Figure 2: Bending of carpenter's tape measure. The total cross-sectional height h narrows down as the tape buckles to a flattened state. This results in a reduced bending stiffness.

level the variation of the cross-section along the beam length is determinant. The stiffness at the end-effector is obtained by taking the inverse of the summed compliances of every infinitesimal beam part. That means that a more compliant segment, e.g. one with small curvature, is lower-bounding the total stiffness and as a consequence it is taking a relatively big part of the deformation. This is a self-amplifying effect, because the more a cross-section is deformed, the more it will tend to a flattened state, thus increasing even more its compliance. It is however possible that the bending threshold at which the transverse curvature flattens is reached at multiple places. In that case the deformation will concentrate at multiple spots.

Another influence that will be taken in consideration in the given design example is the self-weight of the system. The shape of the beam has influence on the distribution of its weight. Since every segment of the beam moves differently, the effect of the shape on the deformation and on the balancing behavior is hard to predict without numerical modelling.

The effect of these local phenomena on the global behavior in combination with non-uniform shapes is hardly predictable by reasoning alone, or by analytical methods. Numerical simulations in combination with shape optimization are therefore applied to deal with those complexities and to

be able to tailor the response of such structures.

2.1.2. Topology and choices

The chosen topology and parametrization (see 2.3.2) are formulated such that the above mentioned phenomena are exploited best: The ability to tailor the in-plane shape of the beam as well as its local transverse curvature.

A schematic representation of the topology is given in figure 3. The shell is defined on a rectangular domain. Two lateral edges are free (green). One transversal edge is clamped (red), and the other one is rigidly connected (blue) to a pilot point P. At the pilot point a vertical displacement D_z is imposed stepwise and the reaction force is retrieved at every step. The pilot point is free to move in the other directions and free to rotate in all directions. The geometry is symmetric in the xz-plane. Moreover the transverse curvature is either concave or convex for every cross-section, i.e. no inflection point, no corrugations.

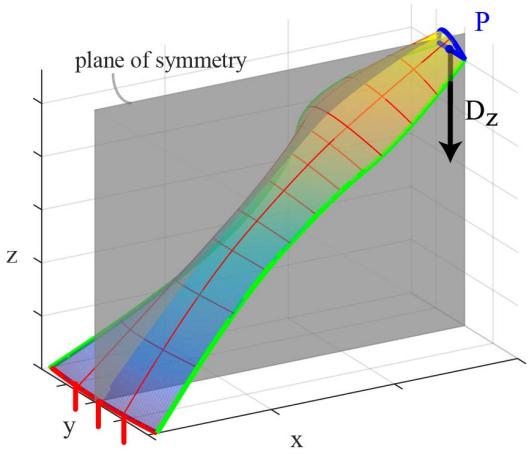

Figure 3: Topology of the compliant shell mechanism. A topologically rectangular patch with a clamped edge and with opposing edge driven by a vertical displacement D_z applied at a rigidly connected control point P. The shape is symmetric in the xz-plane.

2.2. Numerical model

The shell is modeled as a Kirchhoff-Love class Cosserat continuum. Herein a linear and isotropic material law is adopted that also takes the

self-weight into account. Moreover a uniform thickness is assumed over the whole shell surface.

The numerical analysis is based on an isogeometric analysis [44] framework where the parametric descriptions of the geometry of both the design and the analysis are based on non-uniform rational basis splines (NURBS) [45]. The essence is that a relatively low number of control points of a NURBS surface are used as design variables, i.e. optimization variables, and an increased number of control points that describe the *same identical* geometry are employed as degrees of freedom of the numerical analysis. The burden, the time and the loss of continuity that accompanies meshing complex geometries in conventional FEA methods are overcome by the isogeometric discretization. In an optimization procedure where this is repeated a large amount of times, the advantage can be considerable.

B-splines, a uniform and non-rational subset of NURBS, are used in this work. A topologically rectangular set of control points $B_{i,j}$ with $i = 1, ..., n+1$ and $j = 1, ..., m+1$ controls the shape of the mid-surface of the shell. The surface is defined by the tensor product of two B-spline curves using two independent parameters u and v

$$Q(u,v) = \sum_{i=1}^{n+1} \sum_{j=1}^{m+1} N_{i,p}(u) N_{j,q}(v) B_{i,j} \tag{1}$$

where the parameters u and v are defined within the range of the knot vectors, given by

$$U = \left[u_1, u_2, \cdots, u_{p+(n+1)}\right] \tag{2}$$

and

$$V = \left[v_1, v_2, \cdots, v_{q+(m+1)}\right] \tag{3}$$

and where $N_{i,p}$ and $N_{j,q}$, the basis functions of order p and q respectively,

are defined recursively as

$$N_{i,0}(u) = \begin{cases} 1 & \text{if } u_i \leq u < u_{i+1}, \\ 0 & \text{otherwise.} \end{cases} \tag{4}$$

and

$$N_{i,p}(u) = \frac{u - u_i}{u_{i+p} - u_i} N_{i,p-1}(u) + \frac{u_{i+p+1} - u}{u_{i+p+1} - u_{i+1}} N_{i+1,p-1}(u). \tag{5}$$

The basis functions for the v parameter are similar when replacing u, i, p by v, j, q respectively.

The nonlinear solution is found by a standard Newton-Rhapson scheme with position control.

The parametrization of the surface can be refined for the analysis phase by order elevation (p-refinement) and knot insertion (h-refinement) techniques [44]. Without going into detail in these refinement techniques, it is a peculiar fact that the geometry remains perfectly preserved when applying such refinement. This makes it possible to conveniently use different levels of refinement in the subsequent stages of the optimization, incrementing the accuracy as the optimization progresses.

2.3. Optimization

The requirements for the parametrization of the shell model are related to an effective optimization, an accurate simulation and enough flexibility for a high influenceability of the response. For an effective and efficient optimization a low number of parameters is preferable and sensible bounds on the parameters must be possible to formulate. For this purpose a reparametrization of the rectangular set of control points is proposed, which is based on a central line of control points with branches to the sides.

2.3.1. Objective function

A stepwise displacement downwards is imposed on a pilot point P that rigidly transfers all rotations and translations to the upper edge of the shell. The reaction forces are retrieved at all load-steps. The optimization consists in finding the shape for which the force-displacement curve is most constant. The value of the constant force, i.e. the payload, is not considered relevant here. In fact, if the balancer would be able to balance just the self-weight of the shell plus a small payload to be able to fine-tune the behavior in real-life, this would be sufficient. Therefore the objective function is obtained by taking the sum of the absolute value of the deviation between the force F_k at all load-steps with respect to the mean value of this force $\bar{F}$.

Thus the optimization problem is defined as

$$\begin{aligned} &\underset{\mathbf{x}}{\text{minimize}} \quad f(\mathbf{x}) \\ &\text{subject to} \quad \mathbf{b}_l < \mathbf{x} < \mathbf{b}_u. \end{aligned} \tag{6}$$

where $\mathbf{b}_l$ and $\mathbf{b}_u$ are the lower and upper bound vectors, $\mathbf{x}$ is the vector of parameters and f, the objective function, is given by

$$f = \sum_{k=r}^{s} \left| F_k - \bar{F} \right| \tag{7}$$

with s the number of load-steps and r arbitrarily chosen. The steps smaller than r can be discarded because the force will rapidly change before reaching the desired constant force plateau.

2.3.2. Branch parametrization

The starting point for the proposed parametrization is a rectangular B-spline patch with a control net of $3 \times (m + 1)$ control points. The spatial position of the control points is redefined using a branching structure rather than using the Cartesian coordinates of the points in a grid. The branching consists of a middle longitudinal main branch, referred to as the spine, and symmetrical branches starting from the spine in outward direction, referred

to as the ribs, see figure 4. The spine, which connects the middle row of $m+1$ control points, is constrained to the xz-plane due to symmetry of the shell in that plane. The position of the control points is described by using a sequence of lengths of the connecting lines L_j, with $j = 1, ..., m$, and the relative angles between them θ_j. See [43], where a similar parametrization is applied to a planar beam.

At every control point of the spine two ribs are defined that connect to the corresponding control points on the two outer rows. Due to symmetry, the ribs have pairwise the same length, indicated by l_j with $j = 1, ..., m + 1$, and opposite direction with respect to the xz-plane. As an additional constraint to reduce the amount of variables even further, the direction of the ribs is made perpendicular to the preceding line of the spine L_{j-1}. The direction of the ribs can now be described with a single angle α_j. These angles have a major influence on the local transverse curvature of the shell.

The advantages of this parametrization with respect to e.g. the Cartesian coordinates of all control points are a significant reduction of parameters due to symmetry and due to the elimination of less relevant direction parameters. In the Cartesian coordinates of the control points the parameter count amounts to $3 \times (3 \times (m+1))$. In the proposed parametrization the number of parameters is $2 \times m + 2 \times (m + 1)$. If, e.g., $m = 4$, the number reduces from 45 to 18. Furthermore the parameters can be split in lengths and angles, where the lengths have more influence on the size of sections within the shell and the angles affect the local curvature the most. The spine angles θ_j affect the longitudinal curvature and the rib angles α_j affect the local transverse curvature most. This facilitation of the physical interpretation of the design variables has advantages when designing an initial guess and sensible bounds for an optimization run, and for the interpretation and comparison of results after optimization. Moreover, it is possible to add less impacting parameters, e.g. the lengths, in a later stage of the optimization, as will be discussed in section 2.3.3.

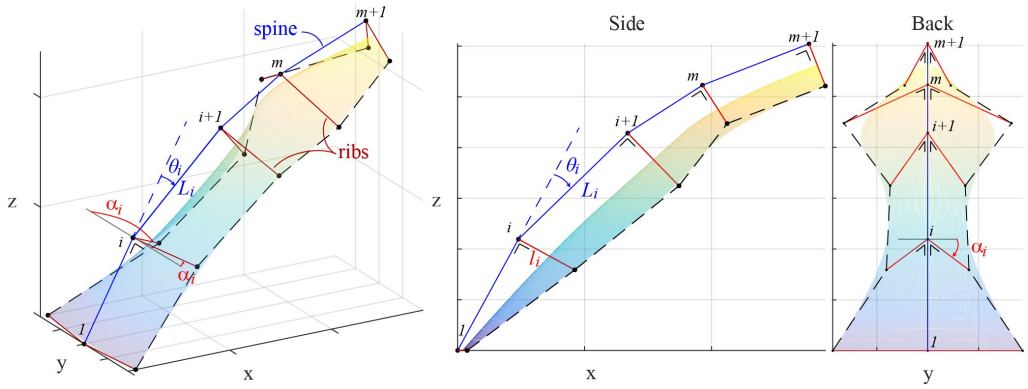

Figure 4: The reparametrization of the B-spline control net is defined by a middle main branch, referred to as the spine, and side branches, referred to as the ribs. The shape of the B-spline surface is defined by the lengths and the relative angles of the spine and ribs segments. This parametrization facilitates the physical interpretation of the design variables and the application of optimization bounds.

2.3.3. Stepwise optimization

Optimization of a shell shape including nonlinear behaviors can be a costly task. Moreover, if the problem is not convex, but in fact has many local optimum solutions, searching for a good solution is even harder.

A stepwise approach is adopted where an initially large population of initial guesses is optimized with a course refinement and a relatively low number of design parameters, i.e. some parameter values have been fixed. While the population size is reduced by selecting the best candidates, the level of refinement and the number of parameters is increased. This stepwise process is illustrated in table 1.

At the first step a large set of design vectors is randomly distributed over the bounded search space and evaluated once. A selection of best performing candidates continues the procedure using an unbounded Nelder-Mead Simplex algorithm (Matlab® fminsearch). This is a gradient free algorithm that handles discontinuities and bumpyness of the objective function decently. In the subsequent steps the optimization is continued by adding the segment lengths to the list of parameters, increasing the number of degrees of freedom and orders of the basis functions. At each step the population

size is reduced by selecting the best candidates from the previous step.

No additional optimization constraints were employed to prevent excessive stress levels. However, between the steps it is possible to check the stress levels in the selected candidates, and in case of excessive stresses the thickness of the shell can be adapted. The subsequent optimization step is likely to correct the resulting change in objective function value. This is only a feasible strategy since the magnitude of the resulting force does not matter, i.e. the important thing is that static balance results.

step	pop.	des. params.	order p and q	DoFs
1	5000	θ_j, α_j	3 3	300
2	50	θ_j, α_j	3 3	300
3	25	θ_j, α_j, L_j, l_j	3 3	300
4	12	θ_j, α_j, L_j, l_j	4 4	483
5	3	θ_j, α_j, L_j, l_j	4 4	2040

Table 1: Stepwise optimization: In five subsequent phases the initial population is reduced from 5000 candidates to 3 best solutions. In the process the number of degrees of freedom, the number of parameters and the order of the basis function are gradually increased.

3. Results

The best three results of an optimization run are presented in this section. The results are based on the following input details. The knot vectors of the bivariate B-splines describing the surface geometry are uniform vectors, given by

$$U = \begin{bmatrix} 0 & 0 & 0 & 1 & 1 & 1 \end{bmatrix} \tag{8}$$

and

$$V = \begin{bmatrix} 0 & 0 & 0 & 1/3 & 2/3 & 1 & 1 & 1 \end{bmatrix} \tag{9}$$

The full vector of design parameters is given by

$$\mathbf{x} = \begin{bmatrix} \theta_1 \cdots \theta_4 & \alpha_1 \cdots \alpha_5 & L_1 \cdots L_4 & l_1 \cdots l_5 \end{bmatrix} \tag{10}$$

The lower and upper bounds on the vector of design parameters are imposed only during the first step of the stepwise optimization. Here the optimized variables are only the angles θ and α and are all bounded between -1 rad and 1 rad. The lengths of the spine segments en ribs, L_j and l_j, are all set to 0.1 m and 0.05 m respectively. This yields shells with length to width relation of about 4:1. This is done to resemble roughly the thin walled slender beam with varying curvature, following the rationale of section 2.1.1. After the first step, i.e. the random search, all bounds are released and the lengths are set as free variables.

The analyses are performed by applying a downward displacement of 0.4 m in 50 load-steps. The simulated material is PETG (Polyethylene terephthalate glycol-modified) with a Young's modulus of 2.35 MPa, Poisson's ratio of 0.38 and a density of 1300 kg/m3. The chosen thickness is 0.9 mm. This is a rough estimate of the shrinking of a 1 mm sheet in the vacuum forming production process.

The best three results of the optimization are presented in figures 5, 6 and 7. The plots on the left hand side show the vertical forces at the base and at the top of the shell versus the applied displacement. On the right hand side the undeformed shape and the maximally deformed shape are shown. The von Mises strains are shown as colors on the deformed shape.

Furthermore the design vector and the objective value of the three results are given in table 2.

3.1. Convergence analysis

The analysis is repeated with increasing refinement by knot insertion (h-refinement). This is done by inserting equally distributed knots within every non-zero knot span. In the u direction the additional knots are inserted in multiples of six, while in the v direction the knots are inserted in multiples of twenty for every non-zero knot span. The convergence is performed in ten steps for both the 3th order model as for the 4th order model. The details are shown in table 3 where also the resulting number of DoFs is indicated

# 1	# 2	# 3
Objective f		
0.0330	0.0969	0.0422
Design vector $\mathbf{x}$		
-0.1011	-0.6814	-0.6472
0.1173	0.0461	0.0579
-0.1114	0.7841	0.9505
-0.2505	-0.1044	-0.2717
-0.1202	0.0870	-0.1219
1.1895	1.0836	0.6269
-0.1741	-0.4877	-0.3797
-1.2974	0.0795	0.5297
1.3033	0.9035	-0.2627
0.1266	0.0978	0.0920
0.0740	0.1351	0.1463
0.1801	0.1551	0.2126
0.1452	0.1590	0.1720
0.0199	0.0675	0.0304
0.0427	0.0481	0.0336
0.0497	0.0518	0.0468
0.0530	0.0502	0.0202
0.0911	0.0449	0.0462

Table 2: Objective function value f and design vector $\mathbf{x}$ of results #1, #2 and #3 corresponding to figures 5, 6 and 7.

and the relative error with respect to the last result in each series. The error is defined as the root mean square of the normalized error between the force values of the current analysis with respect to the most refined analysis, i.e. step 10. This gives

$$error = \sqrt{\frac{1}{s-r}\sum_{k=r}^{s}\left(\frac{F_{k,step} - F_{k,10}}{F_{k,10}}\right)^2} \tag{11}$$

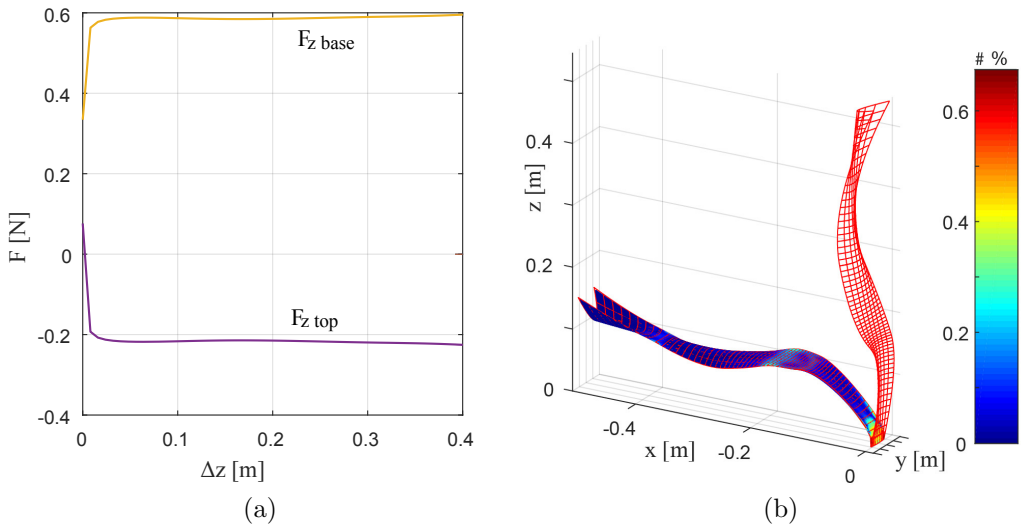

Figure 5: Result#1 (a) Vertical forces at base and top (b) Undeformed shape (wireframe) and von Mises strains on the maximally deformed shape

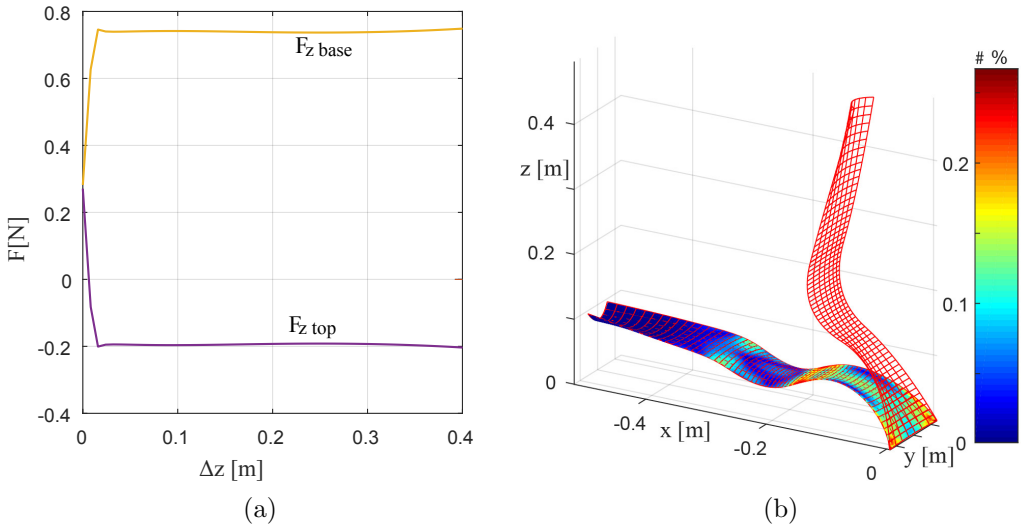

Figure 6: Result#2 (a) Vertical forces at base and top (b) Undeformed shape (wireframe) and von Mises strains on the maximally deformed shape

where *step* is the step in the convergence analysis corresponding to table 3. Figure 8 shows the resulting force-displacement results of the analyses

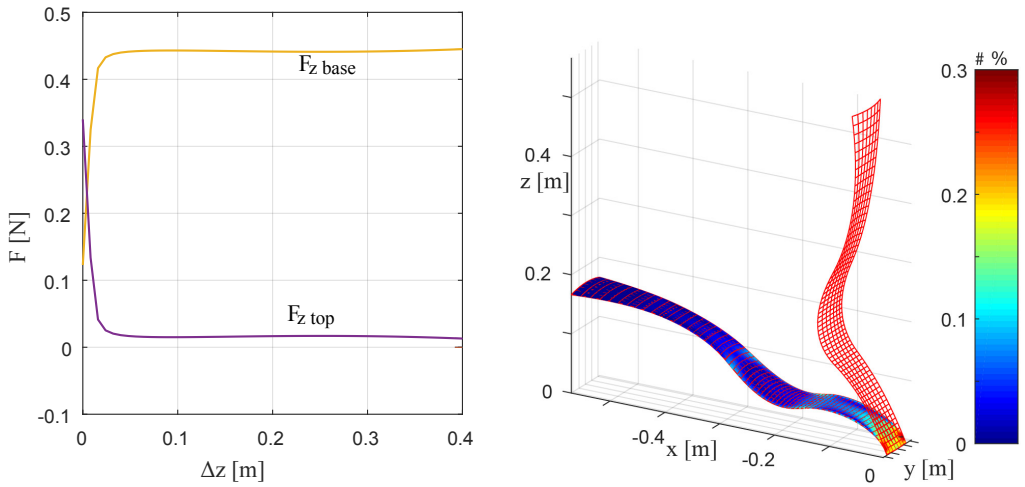

Figure 7: Result#3 (a) Vertical forces at base and top (b) Undeformed shape (wireframe) and von Mises strains on the maximally deformed shape

before and after the convergence analysis.

Observe that control points in this IGA formulation have three degrees of freedom, i.e no rotations. The number of DoFs is thus the number of control points in both direction times three.

4. Physical Model

A physical model was constructed out of PETG thermoplastic sheet material. The shell was made by vacuum-forming the sheet over a high-density foam CNC-milled mold. This is an accessible, quick and cheap manufacturing method. The sheet was trimmed manually at the edges of the shell. The designed shell shape is extended at its bottom edge in order to be able to clamp it to a ground structure, see figure 9a. The ground structure consists of an aluminum clamping unit that presses two 3d-printed jaws of which the clamping surfaces fit the shell shape. Two cylindrical rods are fastened to the bottom of the clamping unit in order to

step	knot ins./span		3th order				4th order			
			control points		DoFs	error	control points		DoFs	error
	u	v	u	v		[%]	u	v		[%]
1	6	20	9	65	1755	3.54	10	68	2040	1.307
2	12	40	15	125	5625	0.602	16	128	6144	0.128
3	18	60	21	185	11655	0.279	22	188	12408	0.063
4	24	80	27	245	19845	0.164	28	248	20832	0.043
5	30	100	33	305	30195	0.106	34	308	31416	0.032
6	36	120	39	365	42705	0.071	40	368	44160	0.024
7	42	140	45	425	57375	0.047	46	428	59064	0.017
8	48	160	51	485	74205	0.028	52	488	76128	0.011
9	54	180	57	545	93195	0.013	58	548	95352	0.005
10	60	200	63	605	114345	0	64	608	116736	0

Table 3: Details of the convergence analysis. The analysis is repeated in ten steps for both the 3th and 4th order basis functions. The refinement is done by inserting equally distributed knots in every non-zero knot span. The insertion is done in multiples of six for the u direction and in multiples of twenty for the v direction.

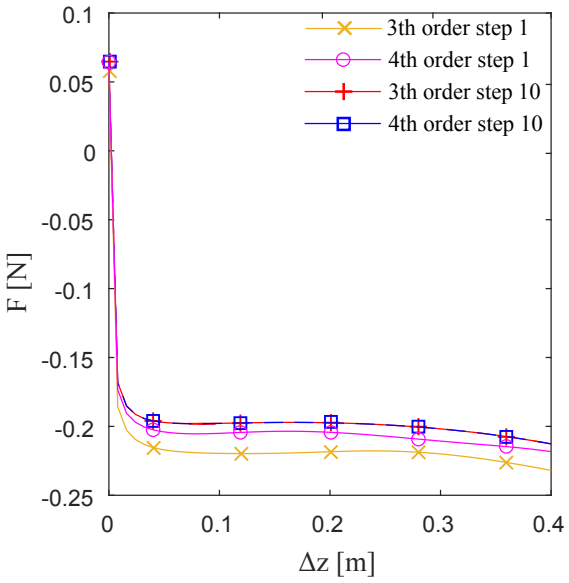

Figure 8: Comparison of force-displacement responses of the numerical results at beginning and end of the convergence analysis.

increase the support polygon of the ground structure. These rods also serve another purpose related to the measurement setup described in section 4.1.

At the opposite side of the shell the edge is trimmed such to include the position of the pilot point P, where the payload can be fixed and where the displacement is applied. Figures 9b and 9c show the clamped shell in the two extreme positions, with and without payload, respectively.

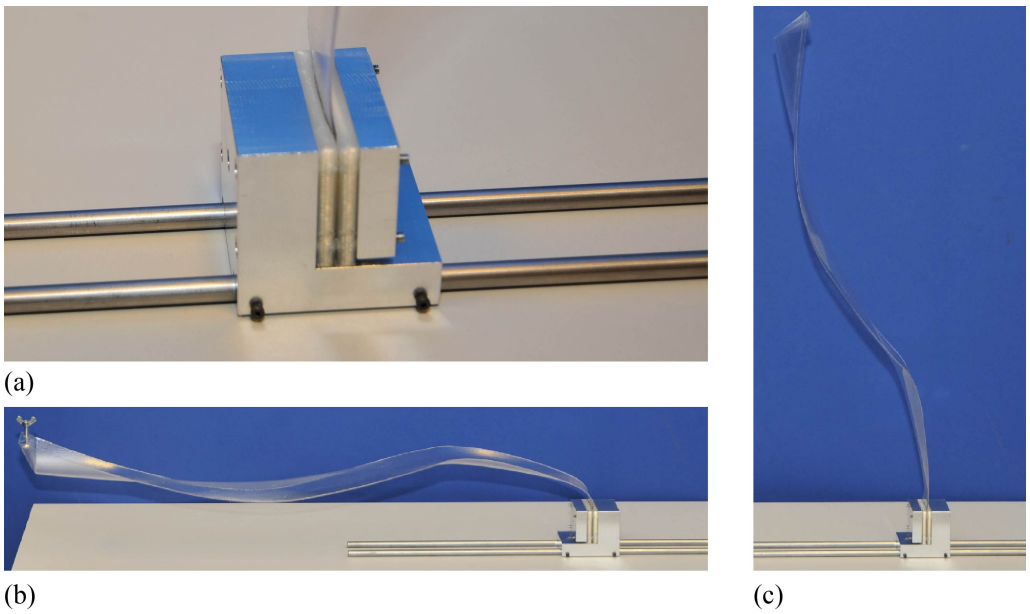

Figure 9: Pictures of the physical realisation of shape #1: (a) Detail of ground structure, (b) loaded shell in maximum deformation, (c) unloaded shell.

4.1. Measurement setup

For the measurement of the vertical reaction force it is important to apply only a vertical displacement while not restraining any motion in the horizontal plane. Since conventional compression benches apply a vertical displacement but do constrain the motion in the horizontal directions, it is possible to position the ground structure on a low-resistance planar stage. This is accomplished here by positioning the base on three pairs of cylindrical rods configured pairwise perpendicular to each other so that they can roll over each other in the two orthogonal directions with no more then the rolling resistance of hardened steel in point contact, i.e. very low. Figure 10 illustrates that pair of rollers number 2 facilitates rolling in the x-direction,

which is the main direction of motion. Pair number 1 is fixed to the aluminum clamp and is used to extend the range of motion of the other rods and to assure a Hertzian point contact. Roller pair number 3 facilitates the motion in y-direction, i.e. perpendicular to the main direction of motion. Although from the numerical models and because of symmetry this component of motion is not expected, in a physical realization with all types of possible errors in fabrication, alignment and material unknowns, such motion cannot be excluded a priori and must therefore be allowed. A last degree of freedom in the horizontal plane that should not be restricted is the rotation. As can be observed in figure 11a the interface between the force sensor and the shell is equipped with a loose vertical screw and a magnet. Rotations in the horizontal plane are easily accommodated. Moreover a small split tube is clamped onto the shell at the position of the pilot point. This ensures that the force sensor which applies the displacement does not restrict the rotation in the direction of the y-axis, at that point.

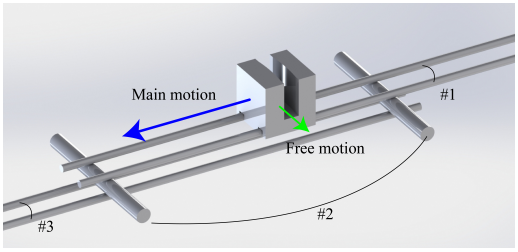

Figure 10: Schematic of the ground structure resting on a planar stage based on three pairs of perpendicular rollers permitting motion in x and y direction.

The displacement is applied by a compression test bench (Testometric M250-2.5CT) with an accuracy of 0.001 mm. The force is measured with a Futek 9N load cell (JR S-Beam Load Cell FSH00092). The travel speed was varied to asses the influence of dynamic effects on the results. The shown results are obtained with 100 mm/min travel speed, at a sampling freuency of 1000 Hz.

The production process has an effect on the thickness of the product that is difficult to predict. This is caused by the stretching of the sheet when

(a)

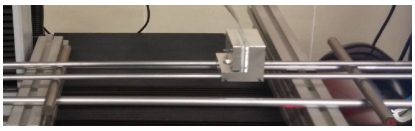

(b)

Figure 11: Detail pictures of measurement setup. (a) The application of the vertical displacement from the test bench goes through a magnet and a rolling tube, allowing for both rotations about the x and z axis. (b) Ground structure resting on the planar stage based on perpendicular rollers.

formed over the mold. As the sheet stretches out the thickness reduces. The thickness of the shells is measured at multiple sampling points using a digital thickness caliper.

4.2. Measurements results

Figure 12 shows the results of the force measurements. Two identically fabricated shells were tested under the same conditions. The signal from the load cell is filtered with a moving average filter (function *smooth* in MATLAB). Both the unfiltered as the filtered results are shown in transparent and opaque lines respectively. The blue lines represent the force for sample 1 in both downward and upward motion direction. The green line shows the same for the sample 2. The force from the optimization result is plotted for reference in red.

Figures 13a and 13b show the thickness distribution of both samples at

selected locations on the shell. The thickness is given in hundreds of a millimeter.

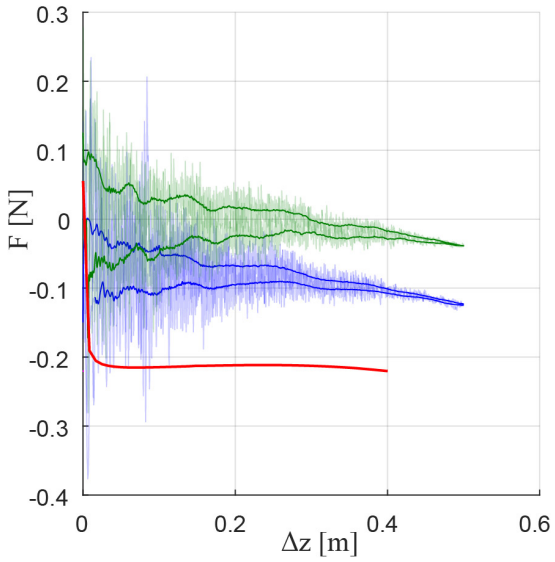

Figure 12: Measurements result. The vertical force at the top of the shell is plotted for the two samples, green and blue, and both unfiltered and filtered, transparent and opaque respectively. The red line shows the result of the optimization, for reference.

5. Discussion

This section is subdivided in categories discussing first the opportunities for generalization of the obtained results, the numerical analysis and optimization, the results and finally the physical model.

5.1. General

It is a general trend to make use of nonlinear effects such as buckling in designing resilient structures. The presented approach and results illustrate the potential of shape optimization to obtain tailored responses. The presented work shows a case study where a constant force is obtained as a result of the double curved complex shape of the shell. This illustrates

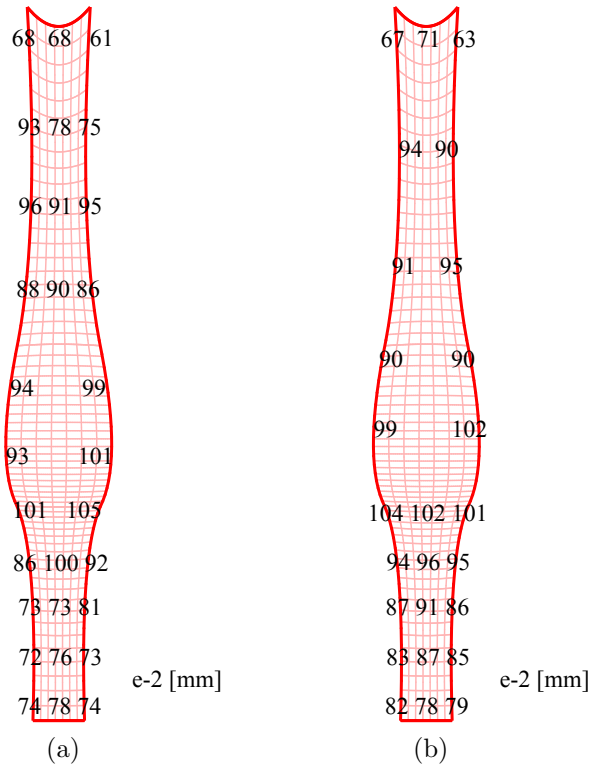

Figure 13: The thickness of the physical model is measured locally at multiple spots to show the influence of the production method on the output of the physical model. (a) and (b) show the thickness values for the two samples at the corresponding locations.

the potential of shells as integrated nonlinear force generators. We have no reasons to assume that other behaviors, including negative stiffness, can not be accomplished by this approach.

Beyond the application of shells as nonlinear force generators, i.e. springs, it is expected that shells with a properly designed and optimized shape can serve more general purposes as mechanisms. While a spring can be defined as a mechanism of which the input and output are at the same location, as suggested by Vehar [5], a general mechanism can be defined as a system transforming motion, energy and/or force, with an input and an output, not necessarily at the same location. A compliant shell mechanism can be employed as a mechanism, taking advantage of the possibility to tailor the

elastic response even further with respect to planar compliant mechanisms.

In current work we have considered only symmetric geometries and loading conditions. Even though the motions out of the symmetry plane were not constrained (only vertical displacements were applied), no measures were taken to stimulate the optimizer to seek such behaviour. Allowing asymmetric shapes could result in interesting constructions with the same type of objective but with asymmetric motions. Asymmetry could be achieved by simply adding a noise on the location of the control points, adding no additional design variables, or by allowing truly asymmetric shapes by increasing the number of design variables. That way also effects as lateral and torsional buckling can be exploited beneficially.

5.2. Numerical model and optimization

The use of isogeometrical analysis for the shape optimization has lead to satisfactory results. The results are smooth and the convergence is good. The refinement level used during the optimization already gives a reasonable prediction of the response. After two refinement steps the error already drops under the 0.1%. Knowing the location of stress concentrations it is advisable to apply the refinement only locally, where needed most. In this case that would be near the base of the shell mechanism. This can drastically reduce the number of degrees of freedom and thus the computational time. This has not been done here in order to make the comparison within the steps and within the different orders more clear.

It must be stressed that the choice of the isogeometric formulation is not a necessary condition for the proposed design process. Although the method has some clear advantages when applied to shape optimization, mainly related to shape fidelity, no need for repeated meshing, and computational cost efficiency (see e.g. [46]), it is possible to base the optimization on other available software packages like Ansys or Abacus.

The reparametrization of the cartesian coordinates of the B-spline into a branch topology turned out beneficial. It makes it easy to apply bounds

intuitively, makes results easier to compare and to interpret. Specifically it helps distinguishing parameters that influence the curvature in both longitudinal and transverse direction, and parameters that influence the width and length of portions of the shell.

The numerical model is based on a linear material law. It is generally known that most polymers, including PETG, have a nonlinear stress-strain relation. Because in this work the strain regime is relatively small (¡1%) a linear model was employed. Applying a nonlinear constitutive law should yield improved representation of the physics. However, in that case the trade-off with the additional computational expenses must be taken into consideration.

5.3. Results

The results of the optimization are very satisfactory in terms of achievement of the objective. The three shown examples have all very good constant force output.

In terms of the distribution of stress over the available material the results are less satisfactory. As anticipated in section 2.1.1 the soft parts of the shell tend to attract most deformation. As these portions deform they become flatter and thus softer, therefore amplifying this effect. The result is a lumped deformation even though the shell thickness is not narrowed down at specific regions as is done in conventional lumped compliant mechanisms. It is expected that by introducing an additional cost function to the optimization this negative effect can be mitigated. Such cost function could include a penalty for stress concentrations and reward designs where the stresses are more evenly distributed.

A benefit of the illustrated approach is that it provides intrinsic end-function realization. There is no need to build it up from multiple subsystems with sub-functions. In the obtained results it is hardly possible to attribute various sub-functions to various parts of the shell. For example, it is not easy to point out a load-carrying positive stiffness part vs a compen-

sator part with negative stiffness, as is the case in many other compliant constant force generators [19, 18].

5.4. Physical model

The physical model was constructed for a qualitative and quantitative evaluation of the system. The measurements show that the behavior of the shell is as predicted, i.e. a constant force. Quantitatively, however, a large discrepancy between measured and predicted force is observed. Main cause of this discrepancy is assumed to be in the production process. Due to the uneven stretching of the material during the vacuum-forming process, and possibly also the anisotropy that is introduced, the thickness of the shell is non-uniform and significantly different with respect to the modelled shell, as can be verified in figure 13. Therefore this experiment cannot be used for validation of the numerical model, but rather only for a qualitative, conceptual validation of the design.

For a successful realization of a shell mechanism it is crucial to obtain a better match between numerical and physical model, taking into account the effects of the production process. It is therefore recommended to invest in the ability to obtain uniform thickness shells, or to integrate the production related effects into the numerical model and accommodate for variable thickness and eventual anisotropy.

The roughness and the hysteresis of the measured force express the difficulty to measure such small forces on such a large travel range, and in particular to measure only the vertical force without influencing the other loading directions. Part of the noise in the results is due to dynamic vibrations of the shell which were observed during the measurements. Another cause of noise and hysteresis is the resistance of the planar stage. Although the resistance is low, is does introduce some small stick-slip disturbances which in turn induce the dynamic vibration. It can be noticed that the noise and the hysteresis is significantly bigger at the begin of the range of motion with respect to the end of the range. That is because initially a small vertical displacement results in a large horizontal displacement of the

base, while at the end the vertical displacement results in almost no horizontal displacement. This brings the hysteresis and vibration in relation to the imperfections and friction caused by the rollers.

6. Conclusions

The design of a gravity balancing compliant shell mechanism with help of shape optimization lead to multiple results with good balancing quality. To the authors' knowledge, the shown results are first of a kind in the design of an irregular shell shape that exhibits a tailored force-displacement response.

The results give confidence that more general mechanism functions can be achieved by spatial, doubly curved structures with large deformations, i.e. compliant shell mechanisms.

Shape optimization as a design tool provides results with intrinsic end-function realisation. Instead of realizing a desired output from the connection of subsystems with dedicated sub-functions, the desired output is tailored at once in the optimization procedure.

A selected design was validated with a convergence analysis. Furthermore two physical models were built and tested. The physical models show qualitatively comparable behavior, but the measurements reveal substantial quantitative discrepancies. The discrepancies, however, can at least partially be explained by the manufacturing uncertainties of the vacuum-forming process and the side effects of the measurement method. As a consequence of the built-in static balancing, both the physical models can be operated with very little effort.

Acknowledgment

The authors would like to acknowledge STW (HTSM-2012 12814: ShellMech) for the financial support of this project.

[1] L. L. Howell, Compliant Mechanisms, John Wiley and Sons Inc., New York,US, 2001.

[2] M. Fox, M. Kemp, Interactive architecture, 1st Edition, Princeton Architectural Press, New York, 2009.

[3] Robotic Building(s), Next Generation Building 1 (1). doi:10.7564/14-NGBJ8.
URL http://default.portal.igpublish.com/iglibrary/browse/journal/article/NGBJ0000010.html

[4] C. A. Mattson, Synthesis through Rigid-Body Replacement, John Wiley & Sons Ltd, 2013, pp. 109–121. doi:10.1002/9781118516485.ch8.
URL http://dx.doi.org/10.1002/9781118516485.ch8

[5] C. Vehar-Jutte, Generalized Synthesis Methodology of Nonlinear Springs for Predescribed Load-Displacement Functions, PhD Thesis, The University of Michigan, Michigan, USA (2008).

[6] K. A. Seffen, Compliant shell mechanisms, Philosophical Transactions of the Royal Society of London A: Mathematical, Physical and Engineering Sciences 370 (1965) (2012) 2010–2026. doi:10.1098/rsta.2011.0347.
URL http://rsta.royalsocietypublishing.org/content/370/1965/2010

[7] M. Farshad, Design and Analysis of Shell Structures, Springer Netherlands, Dordrecht, 1992, oCLC: 851372171.
URL http://dx.doi.org/10.1007/978-94-017-1227-9

[8] A. G. Erdman, G. N. Sandor, S. Kota, Mechanism design:: analysis and synthesis. Vol. 1: [...], 4th Edition, Prentice Hall, Upper Saddle River, NJ, 2001, oCLC: 833833048.

[9] J. J. Uicker, G. R. Pennock, J. E. Shigley, Theory of machines and mechanisms, 4th Edition, Oxford University Press, New York, 2011, oCLC: ocn410229121.

[10] L. C. Leishman, M. B. Colton, A Pseudo-Rigid-Body Model Approach for the Design of Compliant Mechanism Springs for Prescribed Force-Deflections, ASME, 2011, pp. 93–102. doi:10.1115/DETC2011-47590.
URL http://proceedings.asmedigitalcollection.asme.org/proceeding.aspx?articleid=1640834

[11] E. G. Merriam, M. Colton, S. Magleby, L. L. Howell, The Design of a Fully Compliant Statically Balanced Mechanism, ASME, 2013, p. V06AT07A035. doi:10.1115/DETC2013-13142.
URL http://proceedings.asmedigitalcollection.asme.org/proceeding.aspx?doi=10.1115/DETC2013-13142

[12] S. Babaee, J. Shim, J. C. Weaver, E. R. Chen, N. Patel, K. Bertoldi, Metamaterials: 3d Soft Metamaterials with Negative Poisson's Ratio (Adv. Mater. 36/2013), Advanced Materials 25 (36) (2013) 5116–5116. doi:10.1002/adma.201370227.
URL http://doi.wiley.com/10.1002/adma.201370227

[13] A. Rafsanjani, A. Akbarzadeh, D. Pasini, Metamaterials: Snapping Mechanical Metamaterials under Tension (Adv. Mater. 39/2015), Advanced Materials 27 (39) (2015) 5930–5930. doi:10.1002/adma.201570262.
URL http://doi.wiley.com/10.1002/adma.201570262

[14] J. L. Herder, F. P. A. v. d. Berg, Statically balanced compliant mechanisms (SBCM's), an example and prospects, in: Proceedings ASME DETC 26th Biennial Mechanisms and Robotics Conference, 2000. doi:DETC2000/MECH-14144.

[15] S. Deepak R, Static balancing of rigid-body linkages and compliant mechanisms, PhD Thesis, Indian Institute of Science, Bangalore, India (May 2012).

[16] A. Stapel, J. L. Herder, Feasibility Study of a Fully Compliant Statically Balanced Laparoscopic Grasper, ASME Conference Proceedings 2 (46954) (2004) 635–643. doi:10.1115/DETC2004-57242.
URL http://link.aip.org/link/abstract/ASMECP/v2004/i46954/p635/s1

[17] K. Hoetmer, G. Woo, C. Kim, J. Herder, Negative Stiffness Building Blocks for Statically Balanced Compliant Mechanisms: Design and Testing, Journal of Mechanisms and Robotics 2 (4) (2010) 041007–1–7. doi:10.1115/1.4002247.
URL http://dx.doi.org/10.1115/1.4002247

[18] N. Tolou, Statically Balanced Compliant Mechanisms for MEMS and Precision Engineering, PhD Thesis, Delft University of Technology, Delft, The Netherlands (Jul. 2012).

[19] A. G. Dunning, N. Tolou, J. L. Herder, A compact low-stiffness six degrees of freedom compliant precision stage, Precision Engineering 37 (2) (2013) 380 – 388. doi:http://dx.doi.org/10.1016/j.precisioneng.2012.10.007.
URL http://www.sciencedirect.com/science/article/pii/S0141635912001729

[20] D. Nahar, T. Sugar, Compliant constant-force mechanism with a variable output for micro/macro applications, in: Robotics and Automation, 2003. Proceedings. ICRA '03. IEEE International Conference on, Vol. 1, 2003, pp. 318–323 vol.1. doi:10.1109/ROBOT.2003.1241615.

[21] H.-T. Pham, D.-A. Wang, A constant-force bistable mechanism for force regulation and overload protection, Mechanism and Machine Theory 46 (7) (2011) 899 – 909. doi:http://dx.doi.org/10.1016/j.mechmachtheory.2011.02.008.
URL http://www.sciencedirect.com/science/article/pii/S0094114X11000425

[22] G. Berselli, R. Vertechy, G. Vassura, V. P. Castelli, Design of a Single-Acting Constant-Force Actuator Based on Dielectric Elastomers, J. Mechanisms and Robotics 1 (3) (2009) 031007.

[23] C.-C. Lan, J.-H. Wang, Y.-H. Chen, A compliant constant-force mechanism for adaptive robot end-effector operations, in: Robotics and Automation (ICRA), 2010 IEEE International Conference on, 2010, pp. 2131–2136. doi:10.1109/ROBOT.2010.5509928.

[24] N. Hu, R. Burgueño, Buckling-induced smart applications: Recent advances and trends, Smart Materials and Structures 24 (6). doi:10.1088/0964-1726/24/6/063001.

[25] J. Lienhard, S. Schleicher, S. Poppinga, T. Masselter, M. Milwich, T. Speck, J. Knippers, Flectofin: a hingeless flapping mechanism inspired by nature, Bioinspiration & Biomimetics 6 (4) (2011) 045001. doi:10.1088/1748-3182/6/4/045001.
URL http://stacks.iop.org/1748-3190/6/i=4/a=045001

[26] A. Pirrera, X. Lachenal, S. Daynes, P. M. Weaver, I. V. Chenchiah, Multi-stable cylindrical lattices, Journal of the Mechanics and Physics of Solids 61 (11) (2013) 2087–2107. doi:10.1016/j.jmps.2013.07.008.
URL http://www.sciencedirect.com/science/article/pii/S0022509613001385

[27] B. H. Coburn, A. Pirrera, P. M. Weaver, S. Vidoli, Tristability of an orthotropic doubly curved shell, Composite Structures 96 (2013) 446–454. doi:10.1016/j.compstruct.2012.08.026.
URL http://www.sciencedirect.com/science/article/pii/S0263822312003923

[28] N. G. Boddeti, X. Liu, R. Long, J. Xiao, J. S. Bunch, M. L. Dunn, Graphene Blisters with Switchable Shapes Controlled by Pressure and Adhesion, Nano Letters 13 (12) (2013) 6216–6221. doi:10.1021/nl4036324.
URL http://pubs.acs.org/doi/abs/10.1021/nl4036324

[29] S. E. Wilding, L. L. Howell, S. P. Magleby, Spherical lamina emergent mechanisms, Mechanism and Machine Theory 49 (2012) 187–197. doi:10.1016/j.mechmachtheory.2011.10.009.
URL http://www.sciencedirect.com/science/article/pii/S0094114X11002035

[30] J. O. Jacobsen, B. G. Winder, L. L. Howell, S. P. Magleby, Lamina Emergent Mechanisms and Their Basic Elements, Journal of Mechanisms and Robotics 2 (1) (2009) 011003–011003. doi:10.1115/1.4000523.
URL http://dx.doi.org/10.1115/1.4000523

[31] J. O. Jacobsen, G. Chen, L. L. Howell, S. P. Magleby, Lamina Emergent Torsional (LET) Joint, Mechanism and Machine Theory 44 (11) (2009) 2098–2109. doi:10.1016/j.mechmachtheory.2009.05.015.
URL http://www.sciencedirect.com/science/article/pii/

S0094114X09001116

[32] J. J. Parise, L. L. Howell, S. P. Magleby, Ortho-planar linear-motion springs, Mechanism and Machine Theory 36 (1112) (2001) 1281–1299. doi:10.1016/S0094-114X(01)00051-9.
URL http://www.sciencedirect.com/science/article/pii/S0094114X01000519

[33] E. A. Peraza-Hernandez, D. J. Hartl, R. J. M. Jr, D. C. Lagoudas, Origami-inspired active structures: a synthesis and review, Smart Materials and Structures 23 (9) (2014) 094001. doi:10.1088/0964-1726/23/9/094001.
URL http://stacks.iop.org/0964-1726/23/i=9/a=094001

[34] L. A. Bowen, C. L. Grames, S. P. Magleby, L. L. Howell, R. J. Lang, A Classification of Action Origami as Systems of Spherical Mechanisms, Journal of Mechanical Design 135 (11) (2013) 111008. doi:10.1115/1.4025379.
URL http://mechanicaldesign.asmedigitalcollection.asme.org/article.aspx?doi=10.1115/1.4025379

[35] H. C. Greenberg, M. L. Gong, S. P. Magleby, L. L. Howell, Identifying links between origami and compliant mechanisms, Mechanical Sciences 2 (2) (2011) 217–225. doi:10.5194/ms-2-217-2011.
URL http://www.mech-sci.net/2/217/2011/

[36] A. D. Norman, Multistable and morphing corrugated shell structures, Thesis, University of Cambridge (Jun. 2009).
URL https://www.repository.cam.ac.uk/handle/1810/244988

[37] M. Schenk, Folded Shell Structures, Ph.D. thesis, University of Cambridge (2011).

[38] K. A. Seffen, S. D. Guest, Prestressed Morphing Bistable and Neutrally Stable Shells, Journal of Applied Mechanics 78 (1) (2010) 011002–011002. doi:10.1115/1.4002117.
URL http://dx.doi.org/10.1115/1.4002117

[39] M. Santer, S. Pellegrino, Compliant multistable structural elements, International Journal of Solids and Structures 45 (24) (2008) 6190–6204. doi:10.1016/j.ijsolstr.2008.07.014.
URL http://www.sciencedirect.com/science/article/pii/S0020768308002989

[40] A. M. Watt, S. Pellegrino, Tape-spring rolling hinges, in: Proceedings 36th Aerospace Mechanisms Symposium, Glenn Research Center, 2002.
URL http://www-civ.eng.cam.ac.uk/dsl/publications/TSR_hinge.pdf

[41] E. Kebadze, S. Guest, S. Pellegrino, Bistable prestressed shell structures, International Journal of Solids and Structures 41 (1112) (2004) 2801 – 2820.

doi:http://dx.doi.org/10.1016/j.ijsolstr.2004.01.028.
URL http://www.sciencedirect.com/science/article/pii/S0020768304000460

[42] S. K. Christine Vehar, Closed-loop tape springs as fully compliant mechanismspreliminary investigationsdoi:10.1115/DETC2004-57403.

[43] G. Radaelli, J. L. Herder, A monolithic compliant large-range gravity balancer, Mechanism and Machine Theory 102 (2016) 55–67. doi:10.1016/j.mechmachtheory.2016.03.015.
URL http://www.sciencedirect.com/science/article/pii/S0094114X16300088

[44] J. A. Cottrell, T. J. R. Hughes, Y. Bazilevs, Isogeometric Analysis: Toward Integration of CAD and FEA, John Wiley & Sons, Chichester, England, 2009.

[45] L. Piegl, W. Tiller, The NURBS Book (2Nd Ed.), Springer-Verlag New York, Inc., New York, NY, USA, 1997.

[46] B. Hassani, S. M. Tavakkoli, N. Z. Moghadam, Application of isogeometric analysis in structural shape optimization, Scientia Iranica 18 (4) (2011) 846–852. doi:10.1016/j.scient.2011.07.014.
URL http://www.sciencedirect.com/science/article/pii/S1026309811001283